Stochastic representation of the microscale spatial variability in thaw depth in permafrost boreal forests

Taro Nakai[1,2], Tetsuya Hiyama[3], Ayumi Kotani[4], Yoshihiro Iijima[5], Takeshi Ohta[4], and Trofim C. Maximov[6]

[1]School of Forestry and Resource Conservation, National Taiwan University, Taipei 10617, Taiwan

[2]International Arctic Research Center, University of Alaska Fairbanks, Fairbanks, AK 99775-7340, USA

[3]Institute for Space-Earth Environmental Research, Nagoya University, Nagoya 464-8601, Japan

[4]Graduate School of Bioagricultural Sciences, Nagoya University, Nagoya 464-8601, Japan

[5]Graduate School and Faculty of Bioresources, Mie University, Tsu 514-8507, Japan

[6]Institute for Biological Problems of Cryolithozone, Siberian Branch of Russian Academy of Sciences, Yakutsk 678891, Russia

Key Points:

- Gamma distribution represented spatial variabilities in thaw depth in two permafrost boreal forests in East Siberia.
- Spatial variability in thaw depth at different thawing stages was modeled using the gamma distribution varying with mean thaw depth.
- A transient layer limited interannual variability of active-layer thickness and alter seasonal progress in spatial variability thaw depth.

Corresponding author: Taro Nakai, `taronakai@ntu.edu.tw`, `taro.nakai@gmail.com`

Abstract

In this study, a simple stochastic representation of the microscale spatial variability in thaw depth in permafrost regions was proposed. Thaw depth distribution measured in the two larch-type forests in eastern Siberia, Spasskaya Pad and Elgeeii, showed different spatial, seasonal, and interannual variability, respectively. Minor year-to-year variation in active-layer thickness was observed in Spasskaya Pad, where a transient layer may constrain further thawing. A gamma distribution accurately represented the thaw depth spatial variability in both sites as the cumulative probability. Thus, a simple model illustrating the spatiotemporal variation in thaw depth as a function of the mean thaw depth was developed using the gamma distribution. A hierarchy of models was introduced that sequentially considered the constant state, linearity, and non-linearity in the dependence of the rate parameter of the gamma distribution for the mean thaw depth. Although the requirements of the model levels differed between Spasskaya Pad and Elgeeii, the proposed model successfully represented the spatial variability in thaw depth at both sites during different thaw seasons.

Plain Language Summary

In permafrost regions, the seasonal thaw depth in the soil is distributed heterogeneously. Depending on the local conditions of the climate, surface, and soil, its distribution varies temporally during the thaw season. Thus, it is challenging to represent the spatial thaw depth distribution using a physical model. If we assume that the thaw depth is distributed randomly in space, the spatial variability can be represented in a stochastic manner. We successfully represented the cumulative probability of the measured thaw depths in this study in two larch forests in eastern Siberia using a gamma distribution. In addition, we developed a model to represent spatiotemporal variability in thaw depth as a function of the mean thaw depth.

1 Introduction

The active layer, the uppermost soil layer above the permafrost, is subject to seasonal freezing and thawing. Many biological, ecological, hydrological, geophysical, and biogeochemical processes occur in the active layer of the permafrost region (Anisimov et al., 2002; Connon et al., 2018; Fisher et al., 2016). Observations of the active layer and near-surface permafrost reveal how they respond to climate change. Intensive mon-

itoring of the end-of-season thaw depth (active-layer thickness, ALT) has been conducted at various locations over long periods, as represented by the Circumpolar Active Layer Monitoring (CALM) program (Brown et al., 2000; Nelson et al., 2004). A grid-sampling design allowed for intra- and inter-site spatial variability analyses, and ALT was highly variable in space and time, even on a microscale (Nelson et al., 1998, 1999; Hinkel & Nelson, 2003; Watanabe et al., 2003). An essential objective of monitoring the spatial and temporal variability in ALT was the determination of spatial representativeness (Brown et al., 2000).

Microscale spatial variability in thaw depth can affect the ecophysiological processes of permafrost forest ecosystems. At the beginning of the 21st century, from 2004 to 2008, a larch forest in Spasskaya Pad in eastern Siberia endured approximately 1.5 to 2 times more precipitation than usual (Iwasaki et al., 2010). During this period, high soil water conditions adversely affected larch tree growth (from 2005 to 2008), damaging and killing some trees (Iwasaki et al., 2010). Yellowing and browning of larch leaves during the growing season (Iwasaki et al., 2010) and significantly reduced sap flow (Iijima et al., 2014) confirmed this observation. Overwet soil conditions and subsequent damage and death of trees reduced the fluxes of water vapor and carbon dioxide in this larch forest ecosystem (Ohta et al., 2014). Most importantly, Iijima et al. (2014) found that damaged and subsequently dead trees were concentrated within a limited area of a 'permafrost valley' with a deeper and oversaturated active layer, even in a small 50 m × 50 m plot. This finding indicated that the frost table microtopography of soil and the resulting soil water redistribution could critically control tree mortality in Siberia's permafrost forest ecosystems under overwet soil conditions.

Larch forest productivity in eastern Siberia is mainly constrained by drought stress in mountainous regions and flooding stress in the plains (Sato & Kobayashi, 2018). Based on these findings, Sato et al. (2020) modified the dynamic global vegetation model, SEIB–DGVM (Sato et al., 2007, 2016). They successfully demonstrated that the soil water redistribution caused by the within-grid elevation heterogeneity increased the mortality risk of larch trees owing to the overwetting of soils at lower elevations. However, the effect of soil frost table microtopography on tree mortality has not yet been implemented in the models, partly because of the difficulty in representing the microscale variability in thaw depth.

The spatial variability in thaw depth is a complex function of soil conditions (texture, components, water/ice content), vegetation, and organic layers. Thus, the deterministic model requires spatial distribution data on environmental parameters that are rarely available (Anisimov et al., 2002). For this reason, Anisimov et al. (2002) proposed near-surface permafrost parameters, including ALT, as randomly spatially distributed variables consisting of both deterministic and stochastic components and developed a stochastic model to represent the ALT mean values and variances, assuming a normally distributed ALT. They showed that the ALT spatial variability measured at several sites in Alaska followed a normal distribution function. The distributions were not highly skewed, indicating that a normal distribution assumption of ALT was sufficient. However, Anisimov et al. (2002) also noted that the Shapiro–Wilk test for normality rejected the null hypothesis of normality in some instances. Therefore, it is uncertain whether a normal distribution adequately represents spatial thaw depth variability. Some thaw depth measurements showed skewed distributions with a long tail on the deeper side, particularly during the early thaw season (for example, Wright et al., 2009; Connon et al., 2018). However, a stochastic representation of thaw depth variability for the early thaw season has not yet been reported. Furthermore, because of soil surface constraints, for the probability distribution for the thaw depth at the shallowest limit, the normal distribution symmetric about the mean might fail to represent the thaw depth spatial variability.

The goal of this study was to represent microscale spatial variability in thaw depth in a stochastic manner. Our study included manual thaw depth measurements at two boreal forest sites in eastern Siberia over several years at different warm-season times. We represent the observed thaw depth variability using a gamma distribution and propose a simple model to represent the spatial variability of thaw depth as a function of the mean thaw depth using the gamma distribution.

2 Materials and methods

2.1 Study sites and experimental design

We measured the spatial distribution of thaw depth in two larch-dominated forests in the middle part of the Lena Basin of the Republic of Sakha, Russia (Fig. 1). The first area was the Spasskaya Pad Scientific Forest Station (62°15′17″N, 129°37′07″E, 214 m a.s.l.; hereafter Spasskaya Pad), situated in a 200-year-old cowberry larch forest (*Larice-*
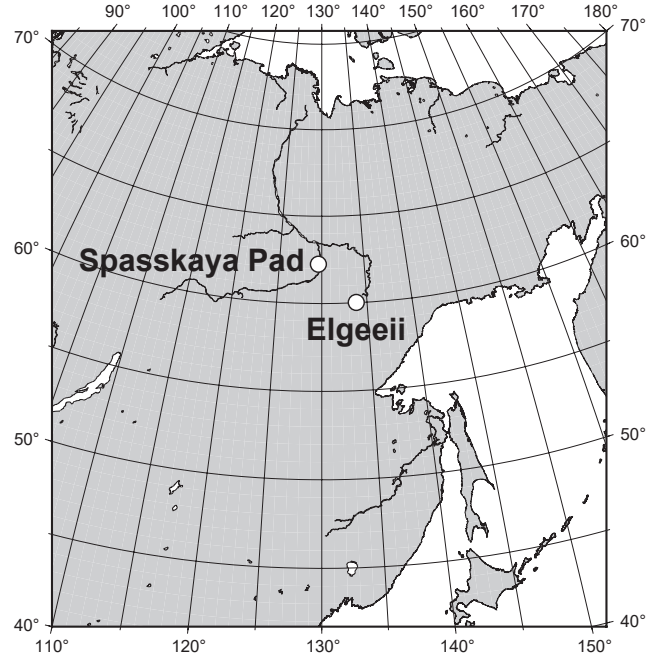
Figure 1. Map showing the locations of the Spasskaya Pad and Elgeeii Scientific Forest Stations.

113 *tum vacciniosum*), located on a Pleistocene terrace on the western bank of the middle

114 sections of the Lena River, approximately 20 km north of Yakutsk city. The second area

115 was the Elgeeii Scientific Forest Station ($60°00'57''$N, $133°49'25''$E, 202 m a.s.l.; here-

116 after Elgeeii) in a highly productive 180-year-old cowberry larch forest located in the third

117 terrace of the left bank of the middle reaches of the Aldan River, approximately 300 km

118 southeast of Yakutsk (Maximov et al., 2019). The mean annual air temperature and pre-

119 cipitation observed at a nearby weather station (Yakutsk Meteorological Observatory)

120 from 1981 to 2010 were -8.7 °C and 236 mm yr^{-1}, respectively (Hiyama et al., 2021).

121 Cajander larch (*Larix cajanderi* Mayr) was the most dominant species at both the

122 sites, followed by silver birch (*Betula pendula* Roth.) and willow (*Salix* sp.) (Shin et al.,

123 2020). Partially, Spasskaya Pad consists of Siberian alder (*Alnus viridis* subsp. *fruticosa*

124 (Rupr.) Nyman) (Shin et al., 2020) and Elgeeii consists of young Scots pine (*Pinus sylvestris*

125 L.) (Kotani et al., 2014). Both sites had similar forest floors that were dominated by cow-

126 berries (*Vaccinium vitis-idaea* L.) mixed with several herbs, such as red baneberries (*Ac-*

127 *taea erythrocarpa* Small), and round-leaved wintergreen (*Pyrola rotundifolia* L.). The Spasskaya

128 Pad also contained water-tolerant grasses, such as narrow-leaved meadow grass (*Poa an-*

Table 1. Periods and numbers of points of thaw depth measurements at Spasskaya Pad and Elgeeii during this study.

Site	Spasskaya Pad		Elgeeii	
Year	Period	Points	Period	Points
2016	4–6 Jul	17[a]	23–24 Jun	17[a]
	24–26 Sep	25	17–18 Sep	25
2017	15–16 Jun	25	6–8 Jun	25
	22–23 Jun	20[b]		
	6–10 Sep	25	18–19 Sep	25
2018			30 Sep	25
2019	18 May	25		
	17, 21–22 Aug	25		
	15–16 Sep	18[c]	21–23 Sep	25

[a] Initial measurement design was 17 points.

[b] Extra measurements in addition to the regular 25 points.
[c] Owing to broken penetrometer parts, we were forced to cease the measurements halfway.

gustifolia L.), and reed grass (*Calamagrostis epigeios* (L.) Roth) (Kotani et al., 2014, 2019; Shin et al., 2020). Fig. 2 shows crown projection maps and photographs of these sites.

The soils of Spasskaya Pad are permafrost pale-solodic, based on a light-old-alluvial sandy loam with high sand content and low porosity. In contrast, the Elgeeii soils were permafrost dark-humus pale-slightly solodic soils based on carbonated loam with high silt, medium to thin particle content, and high porosity (Maximov et al., 2019). The humus horizon thickness did not exceed 5 cm on the Spasskaya Pad and averaged 10–15 cm in Elgeeii (Maximov et al., 2019).

Plots of 50 m × 50 m were set up at these sites (Fig. 2). We routinely conducted multipoint thaw depth measurements at 25 points (the points of the closed circles in Fig. 2) at both sites from 2016 to 2019 (with some exceptions; see Table 1). To capture more detailed spatial variability in thaw depth, we conducted thaw depth measurements at an extra 20 points on Spasskaya Pad (the points of open circles in Fig. 2) in June 2017.
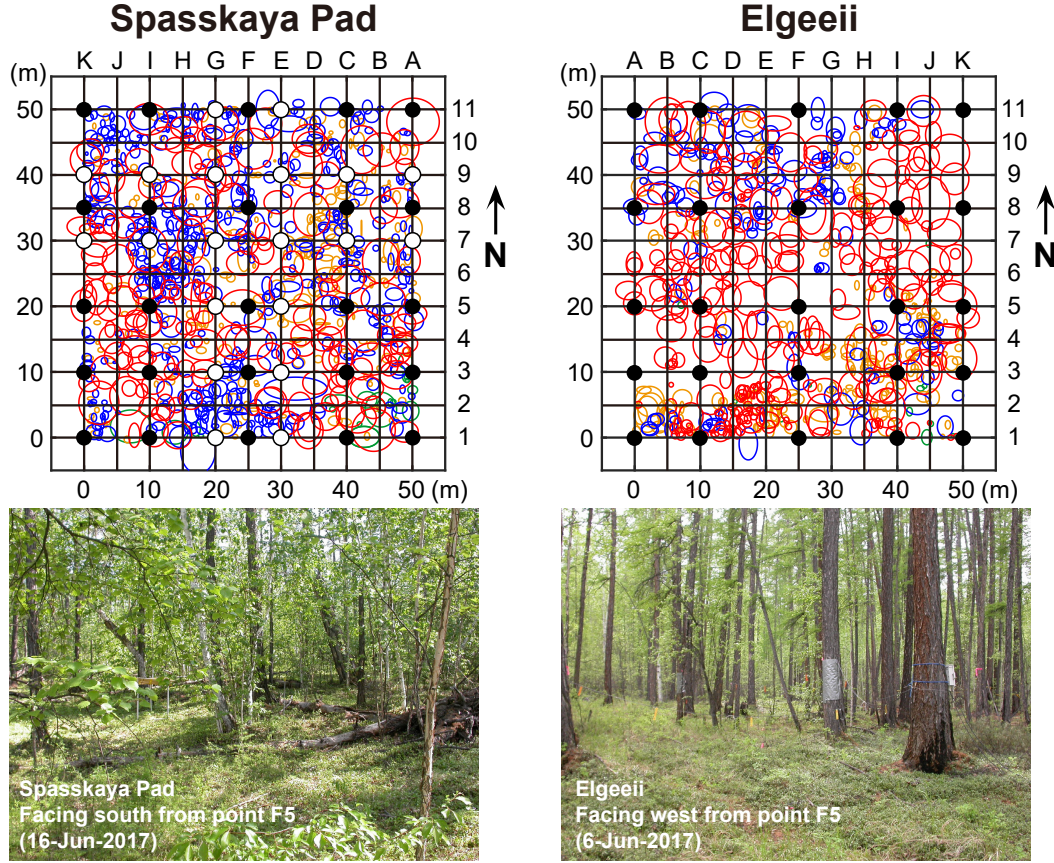
Figure 2. Measurement grids (upper panels) and photographs of forest floor conditions (lower panels) in Spasskaya Pad (left panels) and Elgeeii (right panels). In the grid map, closed circles represent the regular thaw depth measurement points (25 points for each site) and open circles in Spasskaya Pad represent the additional measurement points in June 2017 (20 points). Measurement grids are shown together with the crown projection maps of the study sites: red is Cajander larch (*Larix cajanderi* Mayr.), blue is silver birch (*Betula pendula* Roth.), orange is willow (*Salix* sp.), and green is Siberian alder (*Alnus viridis* subsp. *fruticosa* (Rupr.) Nyman) in Spasskaya Pad and Scots pine (*Pinus sylvestris* L.) in Elgeeii. Crown projection area was measured in 2014 in Spasskaya Pad and in 2008 in Elgeeii.

Figure 3. Photograph of thaw depth measurement using a penetrometer.

₁₄₂ **2.2 Thaw depth measurements**

₁₄₃ We used a handheld dynamic cone penetrometer (TW-035, Sakatadenki Co., Ltd.,

₁₄₄ Tokyo, Japan; hereafter, penetrometer) to minimize uncertainties in thaw depth mea-

₁₄₅ surements. The penetrometer consisted of a tip cone with a 60° angle and a 2.5 cm base

₁₄₆ diameter, guide rod, drive rod with scale, knocking head, and 5 kg slide hammer (Fig.

₁₄₇ 3). The slide hammer free-falling 50 cm along the guide rod strikes the knocking head,

₁₄₈ which drives the cone into the soil. The advantage of this method is that it does not de-

₁₄₉ pend on the physical strength or skill of the measurer, unlike conventional measurements

₁₅₀ using a metal rod. Iijima et al. (2017) confirmed the applicability of a penetrometer to

₁₅₁ measure thaw depths by comparing them with traditional methods (metal rods, frost tubes,

₁₅₂ and soil temperature profiles) at three different sites in eastern Siberia.

₁₅₃ In this study, we used the number of impacts required for 10 cm penetration N_{10}

₁₅₄ as an indicator for determining the thaw depth.

$$N_{10} = \frac{N}{\Delta d_p} \times 10, \tag{1}$$

where N is the number of impacts and Δd_p (cm) is the corresponding increase in penetration depth. The procedure for measuring thaw depth was as follows:

1. The initial depth achieved by the penetrometer's weight was recorded as the initial value.

2. The slide hammer was dropped once (i.e., $N = 1$), and penetration depth Δd_p was recorded.

3. Step 2 was repeated until Δd_p was less than a given threshold ε (e.g., 1 cm).

4. When $\Delta d_p < \varepsilon$, gradually increased the number of impacts N and the corresponding Δd_p were recorded.

5. The depth when N_{10} reached 50 was defined as the thaw depth.

After removing the penetrometer, we inserted a rod with thermocouples into the existing hole and measured the vertical distribution of the soil temperature to determine whether the deepest point reached the frozen soil.

2.3 Analysis of spatiotemporal variability in ALT

The most straightforward way of analyzing spatiotemporal variability in ALT is to directly compare the measured ALT at each grid node over several years. This method shows the absolute interannual variation range of the measured ALT values. However, if the spatial mean ALT varies significantly annually, this may affect the interannual ALT variation range at each grid node.

To examine spatial variability in ALT at individual grid nodes over several years' time series, Hinkel and Nelson (2003) proposed the normalized index of variability I_{v} as follows.

$$I_{\mathrm{v}} = \frac{Z_i - Z_{\mathrm{avg}}}{Z_{\mathrm{avg}}}, \tag{2}$$

where Z_{avg} is the spatial mean ALT for a particular year and Z_i is the node-specific value. Hinkel and Nelson (2003) also defined interannual node variability (INV, presented as %) as the range in I_{v} over several years, that is, the difference between the maximum and minimum values of I_{v} each node over several years. In addition, the grid-mean INV represents the average degree of variability in ALT over the entire recording period (Smith et al., 2009). According to previous results (e.g., Hinkel & Nelson, 2003), Smith et al. (2009) presented a quantitative description of the mean INV as follows: i) *low variabil-*

186   *ity* for sites with the mean INV values of 0–19%, ii) *moderate variability* for sites with

187   a mean INV of 20–29%, and iii) *high variability* for sites with a mean INV of 30% or more.

2.4 Stochastic representation of spatial variability in thaw depth

189   This study adopted the gamma distribution to represent the observed spatial vari-

190   ability in thaw depth. Probability density function (PDF) of gamma distribution $f(x)$

191   for positive variable x is given by

$$f(x) = \frac{\lambda^k x^{k-1} e^{-\lambda x}}{\Gamma(k)}, \tag{3}$$

193   where k is the shape parameter, λ is the rate parameter, and $\Gamma(k)$ denotes the gamma

194   function evaluated at k.

$$\Gamma(k) = \int_0^\infty t^{k-1} e^{-t} dt. \tag{4}$$

196   Notably, $k, \lambda > 0$; therefore, $\Gamma(k) > 0$. The corresponding cumulative distribution func-

197   tion (CDF) $F(x)$ is represented by:

$$F(x) = \int_0^x f(t) dt = \frac{\gamma(k, \lambda x)}{\Gamma(k)}. \tag{5}$$

199   where $\gamma(k, \lambda x)$ denotes the lower incomplete gamma function evaluated at k.

$$\gamma(k, \lambda x) = \int_0^{\lambda x} t^{k-1} e^{-t} dt. \tag{6}$$

201   The advantages of the gamma distribution are that it can be represented by only two

202   parameters, k and λ, and the mean of the distribution is given by k/λ. Because the skew-

203   ness of the gamma distribution is $2/k$, the gamma distribution is positively skewed ($k >$

204   0) and converges with the normal distribution when k is large.

205   The fitting of the gamma distribution to the observed thaw depth data was con-

206   ducted using the R package "fitdistrplus" version 1.1-6 (Delignette-Muller & Dutang,

207   2015; Delignette-Muller et al., 2021). This package was also used for bootstrap analy-

208   sis when determining confidence intervals.

3 Results

3.1 Thaw depth measurements

211   The thaw depth D_T (cm) measured by the penetrometer was confirmed to reach

212   frozen soil based on soil temperature measurements (Fig. 4). In Fig. 4a, the penetrom-

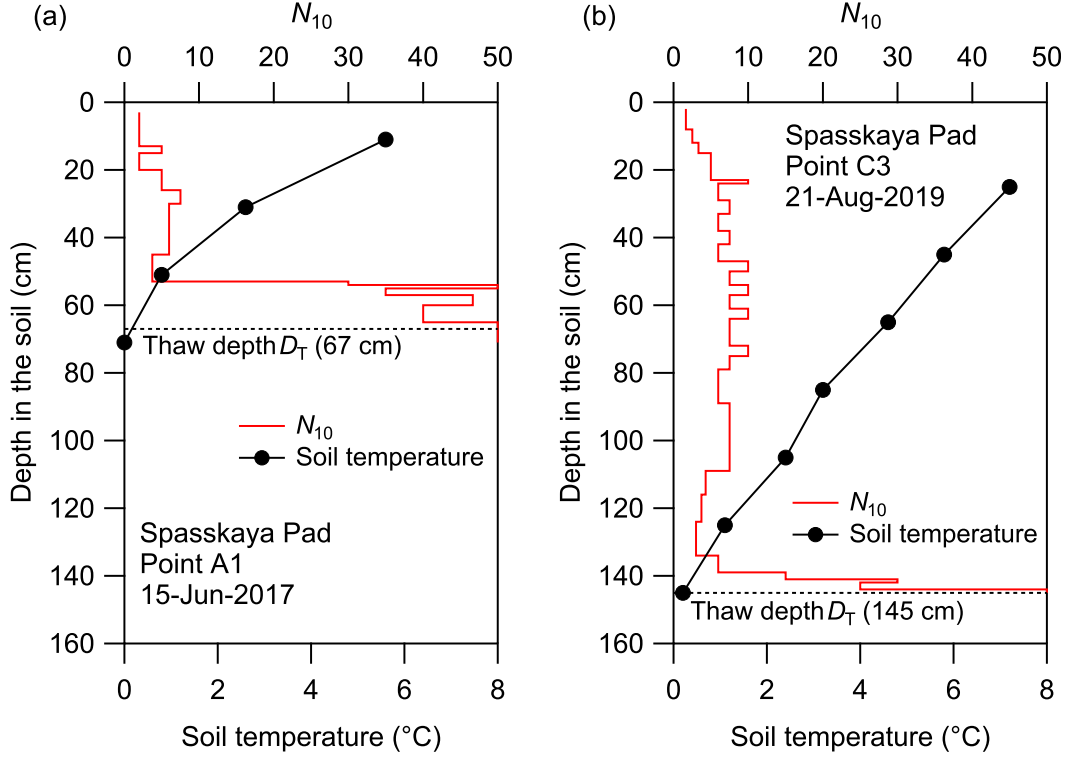213   eter first reached $N_{10} = 50$ at 55 cm depth. However, it encountered the softer soil layer

Figure 4. Plots showing examples of the vertical profiles of N_{10} and soil temperature along with the thaw depth D_{T} determined in Spasskaya Pad. (a) Point A1 in June 15, 2017, (b) point C3 in August 21, 2019.

$(N_{10} < 50)$ thereafter, penetrated another 12 cm, and again reached $N_{10} = 50$ at 67 cm depth. We confirmed that the soil deeper than this point was $N_{10} \geq 50$. According to the soil temperature profile data, the deepest part was confirmed to reach the frozen soil, whereas the first $N_{10} = 50$ depth (i.e., 55 cm) did not. Therefore, we judged the second $N_{10} = 50$ depth (i.e., 67 cm) to be the thaw depth D_{T}. In contrast, in the case shown in Fig. 4b, the penetration depth of $N_{10} = 50$ was determined to reach the frozen soil; thus, it was the thaw depth. These results confirmed that our penetrometer method accurately measured thaw depth.

D_{T} measured at each grid location in September, regarded as the ALT, showed consistent spatial variation in both Spasskaya Pad (Fig. 5a) and Elgeeii (Fig. 5b), irrespective of year. For example, the ALT at location C11 in Elgeeii was always shallower than that at other points (Fig. 5b). This point was located in a depression slightly lower than the others, with high soil moisture and occasional waterlogging. This probably meant that the higher ice content at this point than others necessitated greater latent heat to
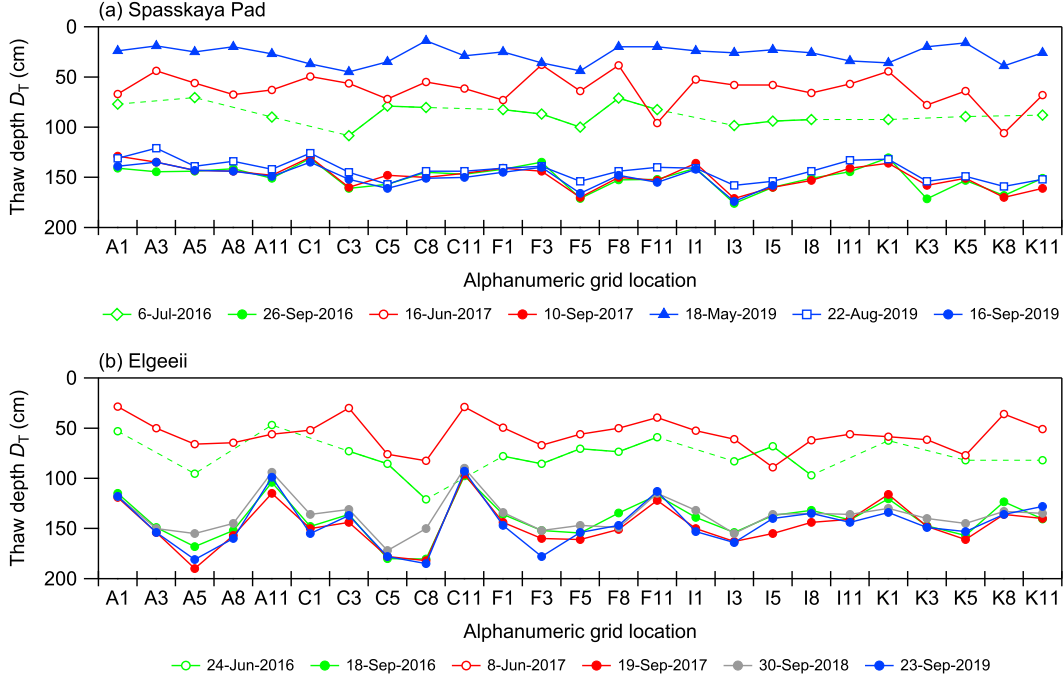
Figure 5. The thaw depth D_T measured at each grid location in Spasskaya Pad (a) and Elgeeii (b).

thaw, resulting in shallower ALT (Clayton et al., 2021). These results indicated that the thaw depths at individual grid points were forced by temperature and various local factors, and the point-specific ALT responded consistently across years, as suggested by Hinkel and Nelson (2003). The consistent spatial variability in ALT over several years was also confirmed by the normalized index of variability I_v (Fig. 6).

The year-to-year fluctuation range of ALT at each point was much smaller for Spasskaya Pad (mean: 5.7 cm, maximum: 13.5 cm) than for Elgeeii (mean: 15.2 cm, maximum: 35.0 cm) (Fig. 5). The INV of Spasskaya Pad was also smaller than that of Elgeeii (Fig. 6c). In Central Yakutia, including Spasskaya Pad, permafrost covered by forests (middle taiga) is known to have a thick (up to 1.0 m) shielding layer (Fedorov et al., 2019; Iijima & Fedorov, 2019). This layer, also referred to as the transient layer (Shur et al., 2005), is located between the base of the active layer and the upper part of the permafrost, contains a sufficient amount of ice, and functions as a buffer between the active layer and permafrost by increasing the latent heat required for thawing. In addition, Spasskaya Pad experienced unusually high rainfall between 2004 and 2008, resulting in increased soil moisture and partial waterlogging. Therefore, we speculated that these overwet soil
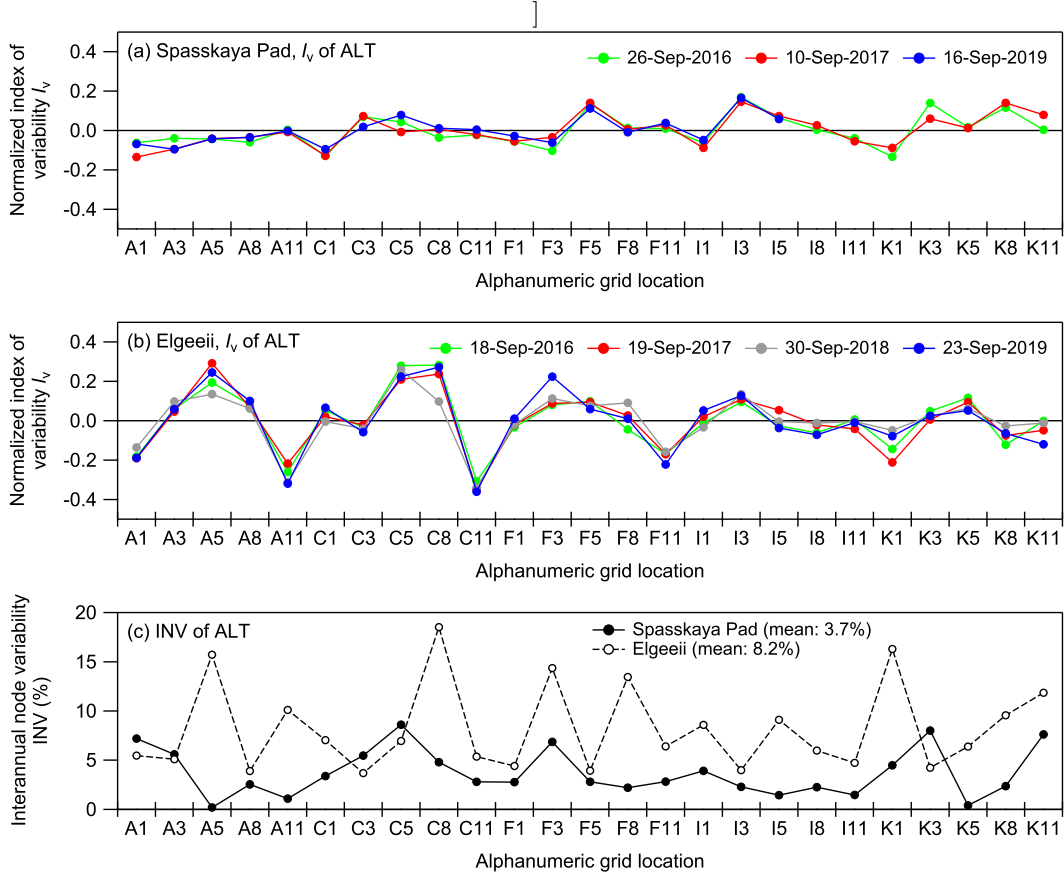
Figure 6. Normalized index of variability I_v of ALT in Spasskaya Pad (a) and Elgeeii (b), and their interannual node variability (INV) in both sites (c).

conditions in Spasskaya Pad enhanced the ice-rich transient layer beneath the active layer, constraining the maximum thaw depth. Despite such differences in the interannual ALT variability between the two sites, grid-mean INV was 3.7% for Spasskaya Pad and 8.2% for Elgeeii, both of which fell into "*low variability*" (Smith et al., 2009).

In contrast, D_T variability during the middle of the thaw period poorly corresponded to ALT variability. Note that we measured D_T near the grid points and were not precise at the same point every time, which would cause inevitable variability in measurements. Nevertheless, considering that such uncertainty also occurs for ALT, this result indicates the processes determining the spatial distribution of D_T during the middle of the thaw periods might be much more complicated than that for ALT.

3.2 Fitting of the gamma distribution

Although the measurements of D_T of each field experiment are distributed heterogeneously and irregularly in space (Fig. 5), sorting these data for each experiment in ascending order represented the cumulative probability distribution, showing a sigmoidal shape (Fig. 7). The distribution pattern differed at each measurement, but the distribution generally ranged wider in Elgeeii than in Spasskaya Pad and became wider when D_T deepened. These results motivated us to represent the spatial variability of D_T in a stochastic manner.

To capture more detailed thaw depth spatial variability, we measured D_T at an extra 20 points in addition to regular measurements at 25 points in June 2017, but the cumulative probabilities of these two D_T were quite different because of about a week interval between the measurements (Fig. 8a). The mean D_T of additional measurements (June 22–23, 2017) was 14.4 cm deeper than that of regular measurements (June 15–16, 2017). Therefore, if we merge these two measurements without correction, the obtained cumulative probability will be erroneous.

Because June is mid-thawing, we assumed that this difference in mean depth occurred during the progress of seasonal thawing. Figure 9 shows the seasonal variation in D_T in 2017 for the Spasskaya Pad. To estimate the seasonal progress of D_T, we adopted the following simplified Stefan equation (Hinkel & Nicholas, 1995).
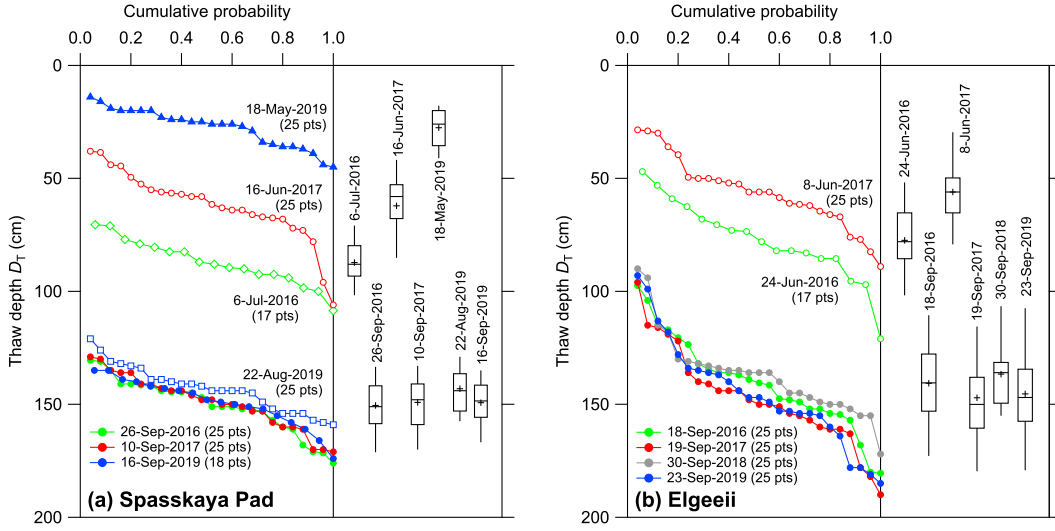
$$D_T = \alpha \sqrt{I_{TS}}, \qquad (7)$$

Figure 7. Cumulative probability distribution of the thaw depth D_T measured at Spasskaya Pad (a) and Elgeeii (b). The boxplots shown together represent the distribution characteristics of the individual measurements, with the box showing the median and the 25th and 75th percentiles, the whiskers showing the 10th and 90th percentiles, and the cross showing the average. The dates shown are representative of each measurement period shown in Table 1.
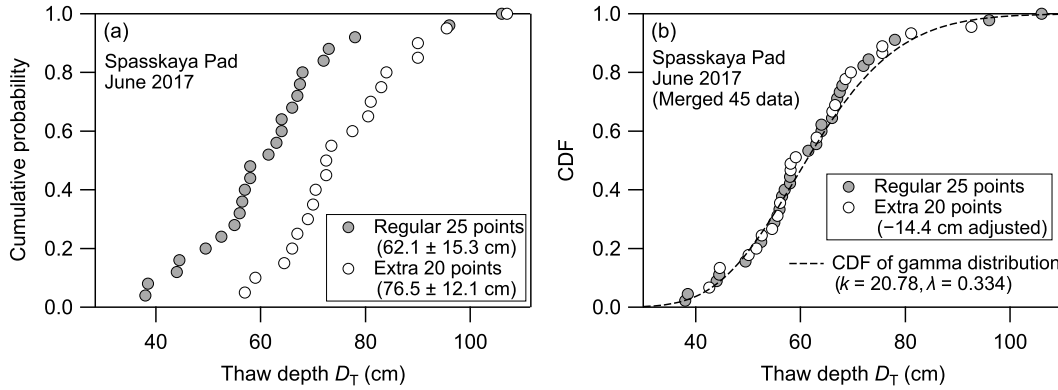

Figure 8. Cumulative probability distribution of thaw depths D_T from regular (June 15–16, 2017, 25 points), and additional measurements (June 22–23, 2017, 20 points) on the Spasskaya Pad. (a) Original data. (b) Merged data using regular measurements and additional measurements adjusted by -14.4 cm. The dashed line in (b) represents the cumulative distribution function of the gamma distribution fitted to the merged data.
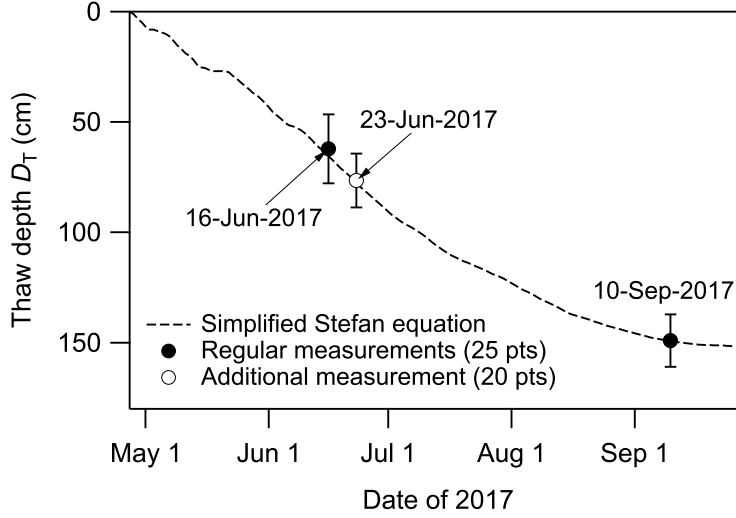
Figure 9. Measured and estimated seasonal variation in thaw depth D_T in 2017 in Spasskaya Pad. The symbols and error bars of measurements show the mean and standard deviation, respectively.

where α is a quasi-constant scaling parameter (cm K$^{-1/2}$ d$^{-1/2}$) that represents the soil's thermal conductivity, density, moisture content, and latent heat effects, and I_{TS} denotes the surface thawing index (K d) calculated by the accumulated degree days of the daily mean surface (0 cm depth) soil temperature measurements above freezing. We determined the α value, such that Eq. (7) matches the measured mean thaw depth $\overline{D_T}$ in September 2017. Both measurements in June agreed well with the estimation by the simplified Stefan equation, implying that the difference between the two measurements was caused by the seasonal thawing progress; thus, the 14.4 cm difference was reasonable. Therefore, we adjusted the additional D_T measurements by -14.4 cm and merged them with the regular ones to create data with 45 measurements for fitting the gamma function.

The cumulative distribution function (CDF) of gamma distribution was in good agreement with the cumulative probability of the merged D_T data (Fig. 8b). The fitting of the gamma distribution was much better than that of the normal and Weibull distributions and similar to other asymmetric distributions (lognormal, Gumbel, and inverse Gaussian; see Fig. S1 and Table S1). Although the fitting of the gamma distribution was not the best of these various distributions, we adopted the gamma distribution in this study because of the advantages mentioned in section 2.4.
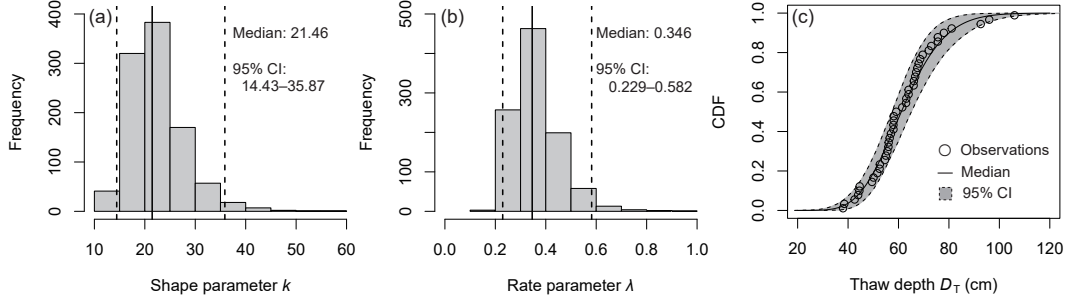
Figure 10. Results of bootstrapping analysis ($n = 1000$) for the merged data in June 2017. (a) and (b) shows the histogram of shape parameter k (a) and rate parameter λ (b) of the gamma distribution, respectively, and (c) shows the cumulative distribution function of the gamma distribution. Continuous and dashed lines represent the median and 95% confidence interval, respectively.

Because the number of measurement points is limited, the fitting of the function inevitably involves sampling uncertainty. For this reason, we conducted a nonparametric bootstrap analysis with 1000 iterations to obtain the 95% confidence intervals (CIs) of k and λ of the gamma distribution. Figure 10 shows the results of the bootstrapping analysis of the merged data in June 2017. The obtained 95% CIs for k and λ were $14.43 \leq k \leq 35.87$ and $0.229 \leq \lambda \leq 0.582$, respectively (Figs. 10a and 10b). As a result, CIs around the CDF of the estimated gamma distribution was constructed (Fig. 10c) with a depth uncertainty of approximately 10–20 cm. The cumulative probability of the merged D_{T} was within this uncertainty. The measured cumulative probability of D_{T} at other times in Spasskaya Pad and Elgeeii was also mainly within the range of uncertainty (Fig. 11). The range of uncertainty in Elgeeii was wider than that in Spasskaya Pad, probably partly because of the wider D_{T} spatial variability in Elgeeii.

3.3 Modeling of spatial variability in thaw depth

The shape parameter k and rate parameter λ showed dependencies on the mean thaw depth $\overline{D_{\mathrm{T}}}$ for both the Spasskaya Pad and Elgeeii (Fig. 12). Using these dependencies, we developed a simple model of representing spatial variability in thaw depth as a function of $\overline{D_{\mathrm{T}}}$. According to the characteristics of the gamma distribution, k is expressed as the product of λ and $\overline{D_{\mathrm{T}}}$ as follows.

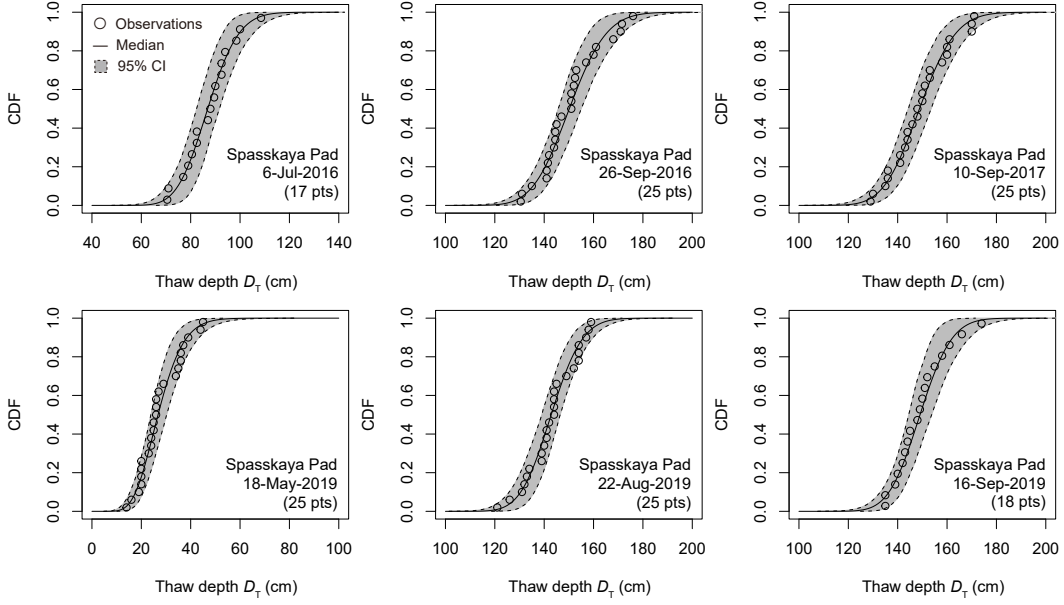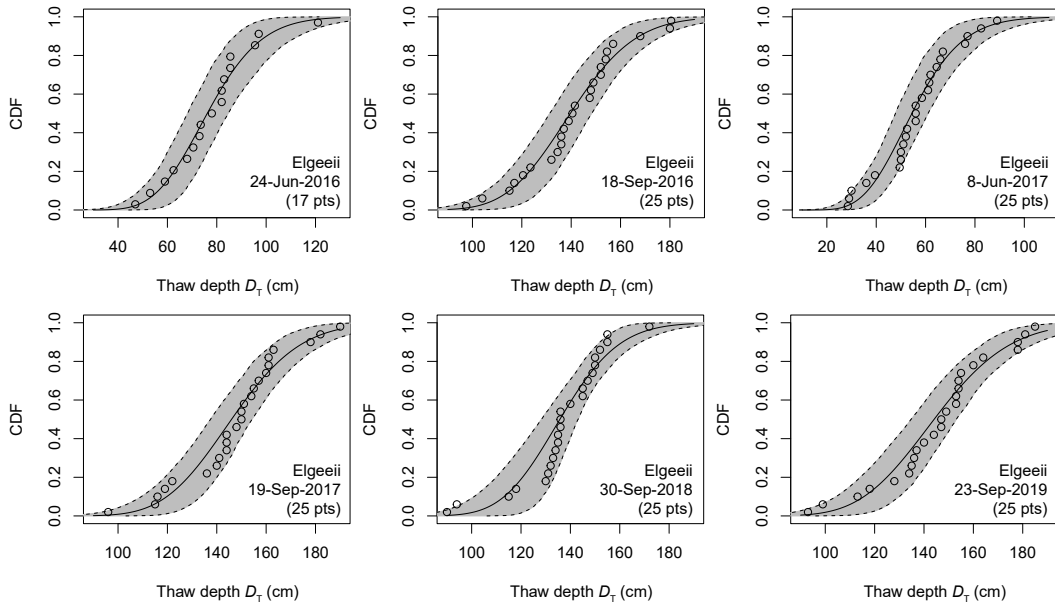$$k = \lambda \overline{D_{\mathrm{T}}} \tag{8}$$

Spasskaya Pad

Elgeeii

Figure 11. Rresults of bootstrapping analysis (n $=$ 1000) for all regular measurements in Spasskaya Pad and Elgeeii other than June 2017 in Spasskaya Pad. The cumulative distribution functions of the gamma distribution are shown. Continuous and dashed lines represent the median and 95% confidence interval, respectively.
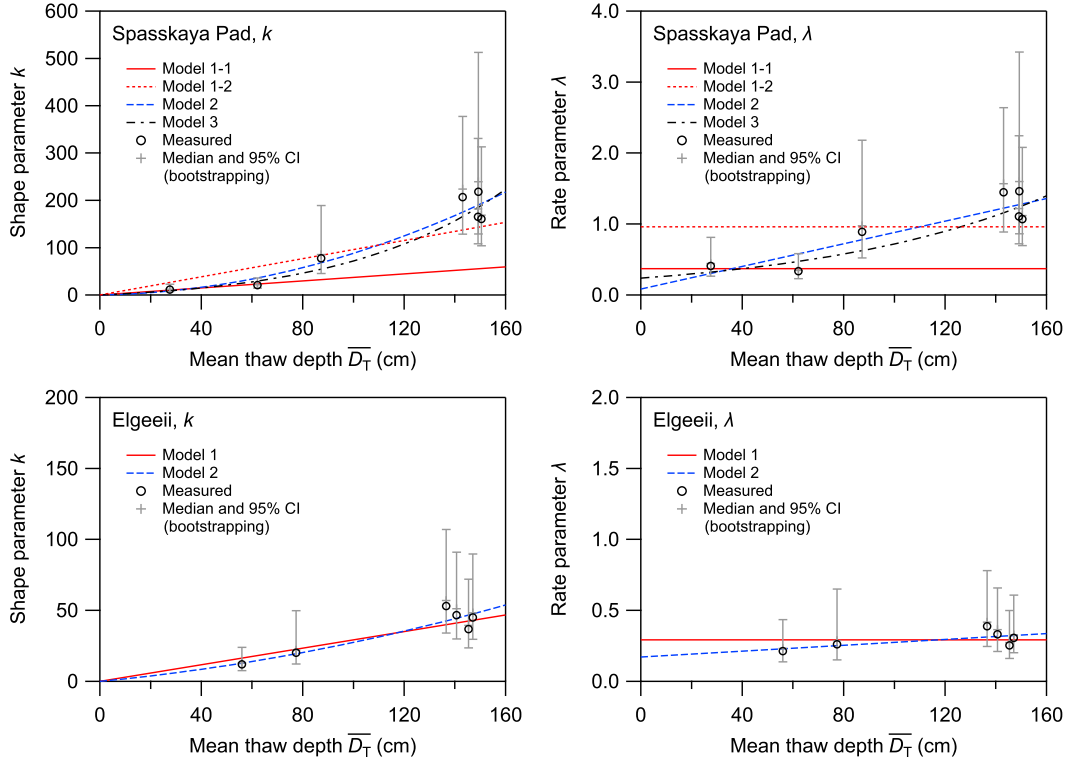
Figure 12. The models of shape parameter k and rate parameter λ in Spasskaya Pad and Elgeeii as functions of the mean thaw depth, $\overline{D_T}$. The measured values, bootstrapping medians, and 95% confidence intervals of k and λ are also shown.

Therefore, we only need to parameterize λ to represent the spatial distribution of thaw depth. Compared with k, λ is less variable against $\overline{D_T}$ (Fig. 12). Using this characteristic, we developed the following three-level models.

Model 1 provides λ as a constant. In this model, k becomes a linear function of $\overline{D_T}$ through the origin. Because λ was less sensitive to $\overline{D_T}$ in Elgeeii, we represented Model 1 for Elgeeii by the mean value of all measured λ.

$$\lambda = 0.292 \quad \text{(Model 1 for Elgeeii)} \tag{9}$$

However, in the Spasskaya Pad, λ increased significantly with $\overline{D_T}$. Large λ values at deep $\overline{D_T}$ may have been caused by the effects of the transient layer. Moreover, a large λ value at $\overline{D_T} = 87.3$ cm (July 2016) may have been possibly caused by the fewer data points (17 points). Note that the λ values measured in May and June were similar and close to the values in Elgeeii's Model 1 (Eq.(9)). Additionally, the λ of June 2017 was the most reliable because it was evaluated from 45 data points and other λ from 25 or fewer data

points. Therefore, if it is not for the transient layer, we expected that λ in May and June would represent all ranges of $\overline{D_T}$. Considering these circumstances, we tested two values for Model 1 on the Spasskaya Pad. Model 1-1 is the mean value of λ measured in May and June, and Model 1-2 is the mean value of all measured λ.

$$\lambda \quad = \quad 0.371 \quad \text{(Model 1-1 for Spasskaya Pad)} \tag{10}$$

$$\lambda \quad = \quad 0.959 \quad \text{(Model 1-2 for Spasskaya Pad)} \tag{11}$$

Model 2 considers the linearity of λ against $\overline{D_T}$. λ generally increased with $\overline{D_T}$ in both Spasskaya Pad and Elgeeii (Fig. 12). Model 2 represents this increasing trend by a linear function. In this model (and Model 3 as well), k becomes a nonlinear function of $\overline{D_T}$ through the origin.

$$\lambda \quad = \quad 7.977 \times 10^{-3} \cdot \overline{D_T} + 0.083 \quad \text{(Model 2 for Spasskaya Pad)} \tag{12}$$

$$\lambda \quad = \quad 1.030 \times 10^{-3} \cdot \overline{D_T} + 0.171 \quad \text{(Model 2 for Elgeeii)} \tag{13}$$

Model 3 considers the non-linearity of λ against $\overline{D_T}$. The λ value in the Spasskaya Pad was significantly larger in September, whereas it was smaller in May and June. Therefore, the linear function cannot represent λ properly for the entire $\overline{D_T}$ range. Furthermore, Model 2 (Eq.(12)) did not represent the most reliable λ of June 2017 evaluated from 45 data points. To represent non-linearly changing λ, including this June 2017 value, we tested a nonlinear function in Spasskaya Pad.

$$\lambda = 0.238 \exp\left(1.106 \times 10^{-2} \cdot \overline{D_T}\right) \quad \text{(Model 3 for Spasskaya Pad)} \tag{14}$$

When fitting Model 3 to the measured λ, the λ in July 2016 was excluded because it had fewer measurements (17 points) and was considered less reliable. We did not test Model 3 for Elgeeii because k and λ in Elgeeii were satisfactorily represented by Models 1 and 2.

In Elgeeii, Model 1 acceptably represented the spatial variability in D_T at different thawing stages (Fig. 13b). Although the cumulative probability of $\overline{D_T}$ measured in Elgeeii had some variability in their sigmoidal shape, the distribution shape and its evolution with depth were reasonably reproduced by both Models 1 and 2. The difference between Models 1 and 2 was subtle; thus, Model 1 was considered sufficient for this site. This result indicates that Model 1 can be used as the first approximation for spatial vari-
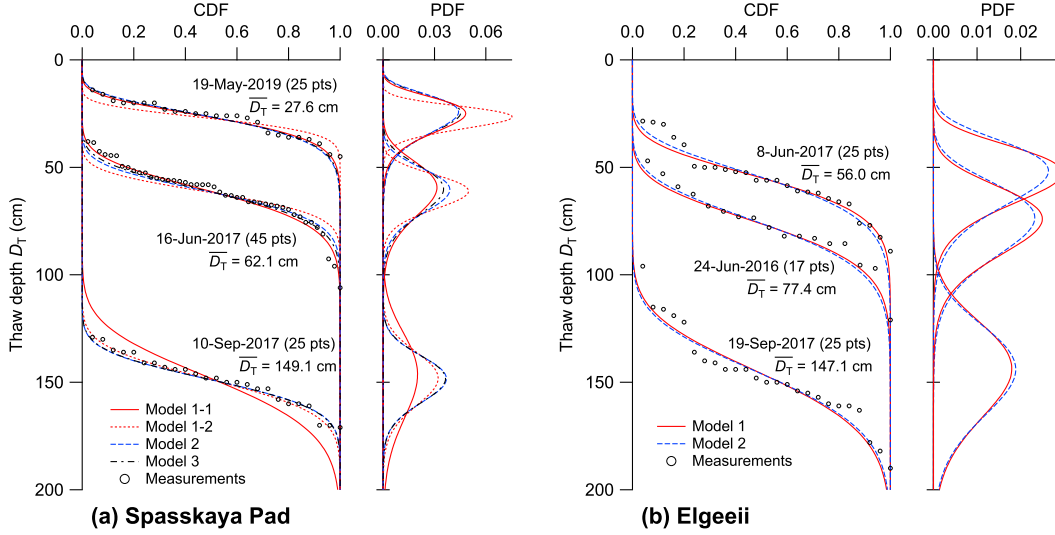
Figure 13. Examples of models of the cumulative distribution function (CDF) and probability density function (PDF) that represent the spatial variability in thaw depth D_T at different timings during the thawing season.

ation in thaw depth at most sites where only the end-season thaw depth (ALT) was obtained.

However, in Spasskaya Pad, both Models 1-1 and 1-2 were insufficient to represent the spatial variability of D_T across the thawing period, and Models 2 and 3 were required (Fig. 13a). Model 1-1 represented the distribution of D_T in May and June reasonably but deviated from the results in September. However, Model 1-2 represented the distribution of D_T measured in September but differed from the results in May and June. If λ is constant, the gamma distribution predicts a gradual increase in the variation range in D_T with increasing mean thaw depth $\overline{D_T}$ because k is proportional to $\overline{D_T}$ (see Eq. (8)) and the variance of the gamma distribution is given by k/λ^2. But in Spasskaya Pad, the range of variation in ALT was similar to that in D_T during the mid-thawing season (Fig. 7a), probably because the maximum thaw depth was restricted by the ice-rich transient layer underneath the active layer. This might explain the discrepancy between Model 1-1 (or 1-2) and the measured cumulative probability of D_T, and why the change in λ should be considered in Spasskaya Pad.
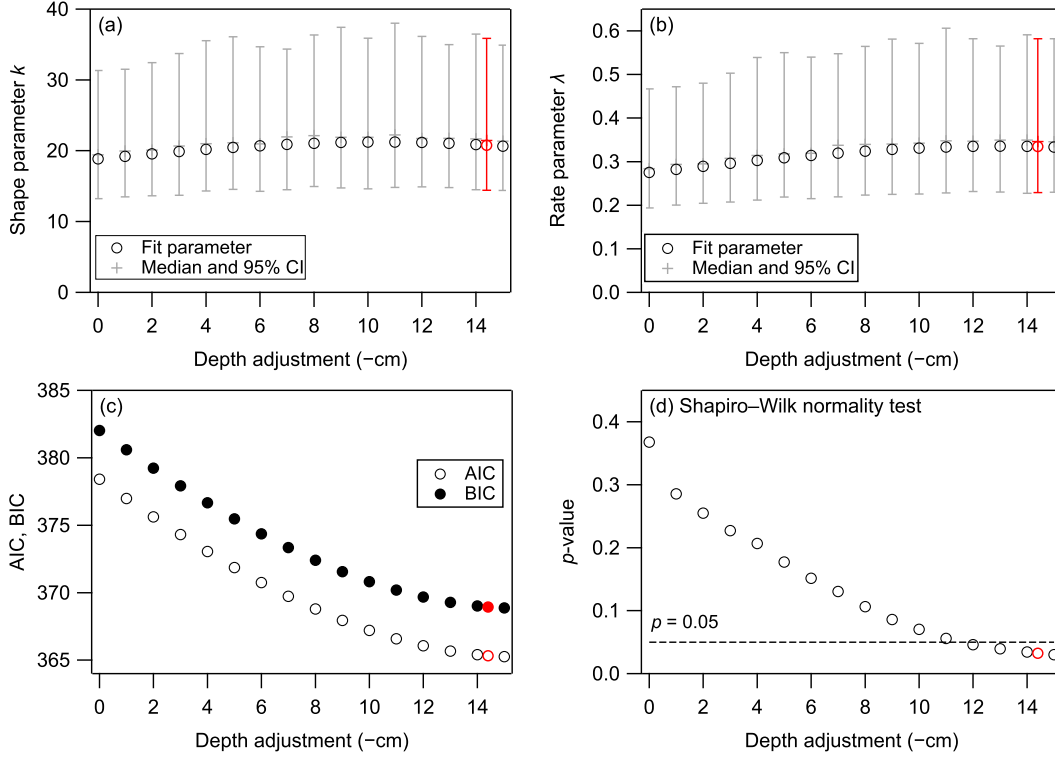
Figure 14. Depth adjustment dependencies for various statistics. (a) Shape parameter k, (b) rate parameter λ, and (c) Akaike Information Criterion (AIC) and Bayesian Information Criterion (BIC) by gamma distribution fitting. (d) The p-value of the Shapiro–Wilk normality test of the dataset. The red-colored markers represent the dataset with a -14.4 cm depth adjustment.

4 Discussion

4.1 Effect of time lag in measurements on statistics

If we measure the thaw depth spatial distribution when the soil thaws rapidly, taking time to measure the multi-point thaw depths D_{T} may produce an inappropriate probability distribution. Because of the one-week time lag between the regular and additional measurements in June 2017, we adjusted the extra 20 data by -14.4 cm in merging the data (section 3.2). To confirm the validity of this adjustment, we analyzed the effect of the depth adjustment on the results using the datasets from June 2017 (Fig. 14).

If depth adjustment is not applied, the shape parameter k (Fig. 14a) and rate parameter λ (Fig. 14b) were slightly smaller than those for the depth adjustment of -14.4 cm. According to the Akaike information criterion (AIC) and Bayesian information criterion (BIC), the gamma distribution fitting score without depth adjustment was the

379 highest (i.e., worst), which gradually declined with increasing depth adjustment (Fig.

380 14c). The -14.4 cm depth adjustment resulted in nearly the best fitting score in this ex-

381 periment. Moreover, according to the Shapiro–Wilk normality test, when depth adjust-

382 ment was -12 cm or larger negative values, the p-value was less than 0.05, i.e., the null

383 hypothesis of normality was rejected (Fig. 14d). Otherwise, the probability distribution

384 of data did not significantly depart from the normal distribution. These results indicated

385 that if the thaw depth measurement takes a long time or is conducted at different times

386 with a specific interval, the obtained uncorrected or unadjusted data may not represent

387 the probability distribution characteristics of the original (or "true") data (e.g., gamma

388 distribution) but rather approach a normal distribution. Therefore, if the thaw depth

389 spatial distribution is measured during the mid-thaw season when the soil thaws rapidly,

390 we highly recommend conducting the measurement for as short a period as possible or

391 adjusting the measured thaw depth.

392 ### 4.2 Effect of plot size on statistics

393 The experimental plots in this study were squares with a side length of 50 m, but

394 it should be noted that thaw depth statistics can be affected by the plot size. To assess

395 the effect of plot size on thaw depth statistics, we calculated the mean, standard devi-

396 ation, and range of distribution (from minimum to maximum) of D_T by changing the

397 plot sizes from 10 m to 45 m at 5 m intervals. Here, the plot size is expressed as the side

398 length of the square plot. For each plot size, all possible non-overlapping combinatorial

399 patterns of grid data within the square frame were considered, using the merged data

400 from June 2017, measured at the 45 grid nodes in the Spasskaya Pad.

401 The plot size dependency of the thaw depth statistics was most pronounced in the

402 range of distribution (Fig. 15). Although the values of the mean (Fig. 15a) and stan-

403 dard deviation of D_T (Fig. 15b) varied significantly when the plot size was small, their

404 average values remained relatively unchanged with respect to the plot size. In contrast,

405 the distribution range significantly increased with plot size (Fig. 15c). This result sug-

406 gests that if the plot size is larger than ours (50 m), the spatial variation in D_T can be

407 even greater. Because of the limited plot size in this study, further investigation of mea-

408 surements from plots of various spatial sizes is necessary to reveal the plot size depen-

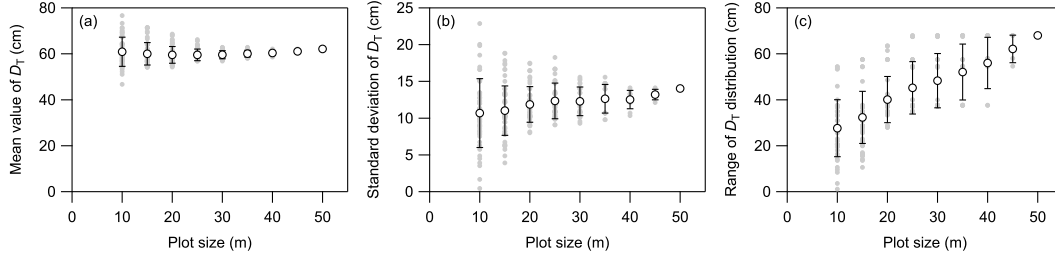409 dencies on a larger scale. Nevertheless, given that the mean and standard deviation of

Figure 15. Plot size dependency of statistics of thaw depth D_T. (a) the mean value of D_T, (b) the standard deviation of D_T, and (c) the distribution range of D_T (i.e. the difference between the maximum and the minimum values of D_T). The plot size is expressed as the side length of a square plot.

D_T were relatively unchanged against the plot scale, the gamma distribution obtained in this study is expected to represent the general characteristics of our research site.

4.3 Effect of sample size on statistics

How many data points are needed to capture the representative spatial variability in the thaw depth D_T is an essential question for field researchers. If we could further increase the sample size, the reliability of the thaw depth spatial variability analysis would be further improved, but the measurement effort would also increase accordingly. In reality, the minimum sample size required to capture the representative spatial variability in thaw depth would be of interest. To assess the minimum sample size, we focused on CIs for k and λ, which we obtained by bootstrapping in Section 3.2. We defined the normalized uncertainty range (NUR) of a parameter as width of 95% CI divided by the value obtained from the observed data. The NUR of k and λ are given as follows:

$$\text{NUR}_k = \frac{k_{97.5} - k_{2.5}}{k_{\text{obs}}} \tag{15}$$

$$\text{NUR}_\lambda = \frac{\lambda_{97.5} - \lambda_{2.5}}{\lambda_{\text{obs}}} \tag{16}$$

where $k_{2.5}$ and $k_{97.5}$ are the 2.5th and 97.5th percentiles of k, $\lambda_{2.5}$ and $\lambda_{97.5}$ are the 2.5th and 97.5th percentiles of λ, and k_{obs} and λ_{obs} are k and λ obtained from the observed data, respectively.

Though the widths of CIs for k and λ varied significantly depending on the timing (mean thaw depth $\overline{D_T}$) and site (see Fig. 12), the relationship between NUR and
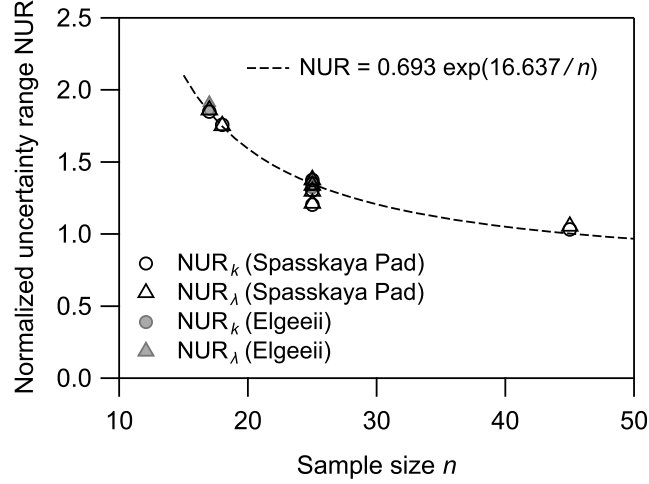
Figure 16. Sample size dependency of the normalized uncertainty range (NUR) for shape parameter k (NUR_k) and rate parameter λ (NUR_λ) in Spasskaya Pad and Elgeeii. The dashed line shows the common curve fitted to all the NUR data represented by an exponential function of the reciprocal of sample size n.

sample size n showed similar characteristics regardless of site, timing, or whether k or λ, which falls along a single common curve (Fig. 16; the numerical data are listed in Table S2). An exponential function of $1/n$, obtained empirically from the relationship between NUR and $1/n$, represented this curve.

$$\mathrm{NUR} = 0.693 \exp\left(16.637/n\right) \tag{17}$$

The NUR with a sample size of $n = 25$ had the highest number of measurements for regular observations and varied more than other sample sizes, ranging from 1.204 to 1.396 including all NUR_k and NUR_λ in the Spasskaya Pad and Elgeeii. However, the mean and standard deviation was 1.331 ± 0.051, showing that most of the data concentrated within a narrow range, around the mean. Figure 16 and Eq. (17) show that the NUR increased as the sample size n decreased. The difference in NUR between $n = 25$ and 45 was relatively small, whereas the NUR was significantly larger when $n = 17$ and 18 compared to others. In other words, uncertainty did not decrease significantly with increasing sample size n when $n \geq 25$, whereas it sharply increased with decreasing n when $n < 25$. This result confirmed that the sample size $n = 25$ for regular measurements in this study was adequate.

The prediction function obtained in this study (Eq. (17)) can be applicable to other sites for uncertainty and sample size assessment. Note that the results in this study were obtained using nonparametric bootstrapping. If parametric bootstrapping is adopted, the obtained results can differ from ours.

5 Conclusions

To simply represent the microscale spatial variability in thaw depth in permafrost regions, this study discussed the applicability of a gamma distribution to the measured thaw depth distributions in two larch forests in eastern Siberia. The thaw depth spatial variability characteristics differed between Spasskaya Pad and Elgeeii, with less variation in Spasskaya Pad, particularly for its seasonal maximum (i.e., active-layer thickness). In Spasskaya Pad, a transient layer underneath the active layer is speculated to constrain the maximum thaw depth.

The gamma distribution well represented the measured thaw depth spatial distribution at both sites with a 95% confidence interval. We found that the shape parameter k and rate parameter λ of the gamma distribution depended on the mean thaw depth. Based on this finding, we developed a simple stochastic model that uses the gamma distribution to represent the spatiotemporal variation in thaw depth as a function of the mean thaw depth. This model consists of three-level models expressing λ dependency on the mean thaw depth. Model 1 represents λ by a constant, Model 2 considers the linearity in λ, and Model 3 considers the nonlinearity in λ. Although the requirements of the model levels differed between the Spasskaya Pad and Elgeeii, the proposed model successfully represented the spatial variability in thaw depth in both sites at different thaw seasons. If the transient layer limits the active-layer thickness, λ significantly increases with the mean thaw depth; otherwise, Model 1 (i.e., constant λ) can be used as the first approximation for the spatial thaw depth variation. This may allow most sites where only the active layer thickness is available to roughly estimate the spatiotemporal variability in thaw depth.

The limitations of this study were that we only measured thaw depth variability in boreal forests, with a limited plot scale of 50 m $\times$ 50 m. Therefore, further investigation is required to discuss the applicability of the gamma distribution and model proposed in this study to sites other than boreal forests, such as tundra, and confirmed the

spatial variability in larger areas. Moreover, our model's coefficients for the rate parameter λ are expected to be represented by other environmental conditions, such as climate zone, soil types, and plant functional types. This may cultivate a further understanding of phenomena and allow robust modeling regarding the active-layer dynamics and their impact on ecological and ecohydrological processes (including carbon, water, energy, and nutrient cycles) in permafrost boreal forests in a changing climate.

References

Anisimov, O. A., Shiklomanov, N. I., & Nelson, F. E. (2002). Variability of seasonal thaw depth in permafrost regions: a stochastic modeling approach. *Ecological Modelling*, *153*(3), 217–227. doi: 10.1016/S0304-3800(02)00016-9

Brown, J., Hinkel, K. M., & Nelson, F. E. (2000). The circumpolar active layer monitoring (CALM) program: Research designs and initial results. *Polar Geography*, *24*(3), 166-258. doi: 10.1080/10889370009377698

Clayton, L. K., Schaefer, K., Battaglia, M. J., Bourgeau-Chavez, L., Chen, J., Chen, R. H., . . . Zhao, Y. (2021, may). Active layer thickness as a function of soil water content. *Environmental Research Letters*, *16*(5), 055028. doi: 10.1088/1748-9326/abfa4c

Connon, R., Devoie, E., Hayashi, M., Veness, T., & Quinton, W. (2018). The influence of shallow taliks on permafrost thaw and active layer dynamics in subarctic Canada. *Journal of Geophysical Research: Earth Surface*, *123*(2), 281–297. doi: 10.1002/2017JF004469

Delignette-Muller, M. L., & Dutang, C. (2015). fitdistrplus: an R package for fitting distributions. *Journal of Statistical Software*, *64*(4), 1–34. doi: 10.18637/jss.v064.i04

Delignette-Muller, M. L., Dutang, C., Pouillot, R., Denis, J.-B., & Siberchicot, A. (2021). Package 'fitdistrplus': help to fit of a parametric distribution to non-censored or censored data [Computer software manual]. (R package version 1.1-6)

Fedorov, A. N., Konstantinov, P. Y., Vasilyev, N. F., & Shestakova, A. A. (2019). The influence of boreal forest dynamics on the current state of permafrost in Central Yakutia. *Polar Science*, *22*, 100483. doi: 10.1016/j.polar.2019.100483

Fisher, J. P., Estop-Aragonés, C., Thierry, A., Charman, D. J., Wolfe, S. A., Hartley, I. P., . . . Phoenix, G. K. (2016). The influence of vegetation and soil characteristics on active-layer thickness of permafrost soils in boreal forest. *Global Change Biology*, *22*(9), 3127–3140. doi: 10.1111/gcb.13248

Hinkel, K. M., & Nelson, F. E. (2003). Spatial and temporal patterns of active layer thickness at Circumpolar Active Layer Monitoring (CALM) sites in northern Alaska, 1995–2000. *Journal of Geophysical Research: Atmospheres*, *108*(D2), 8168. doi: 10.1029/2001JD000927

Hinkel, K. M., & Nicholas, J. R. J. (1995). Active layer thaw rate at a boreal forest site in central Alaska, U.S.A. *Arctic and Alpine Research*, *27*(1), 72–80. doi: 10.1080/00040851.1995.12003098

Hiyama, T., Ueyama, M., Kotani, A., Iwata, H., Nakai, T., Okamura, M., . . . Maximov, T. C. (2021). Lessons learned from more than a decade of greenhouse gas flux measurements at boreal forests in eastern Siberia and interior Alaska. *Polar Science*, *27*, 100607. (Arctic Challenge for Sustainability Project (ArCS)) doi: 10.1016/j.polar.2020.100607

Iijima, Y., & Fedorov, A. N. (2019). Permafrost-forest dynamics. In T. Ohta, T. Hiyama, Y. Iijima, A. Kotani, & T. C. Maximov (Eds.), *Water-carbon dynamics in eastern siberia* (pp. 175–205). Singapore: Springer Singapore. doi: 10.1007/978-981-13-6317-7_8

Iijima, Y., Ohta, T., Kotani, A., Fedorov, A. N., Kodama, Y., & Maximov, T. C. (2014). Sap flow changes in relation to permafrost degradation under increasing precipitation in an eastern Siberian larch forest. *Ecohydrology*, *7*(2), 177–187. doi: 10.1002/eco.1366

Iijima, Y., Park, H., Konstantinov, P. Y., Pudov, G. G., & Fedorov, A. N. (2017). Active-layer thickness measurements using a handheld penetrometer at boreal and tundra sites in eastern Siberia. *Permafrost and Periglacial Processes*, *28*(1), 306–313. doi: 10.1002/ppp.1908

Iwasaki, H., Saito, H., Kuwao, K., Maximov, T. C., & Hasegawa, S. (2010). Forest decline caused by high soil water conditions in a permafrost region. *Hydrology and Earth System Sciences*, *14*(2), 301–307. doi: 10.5194/hess-14-301-2010

Kotani, A., Kononov, A. V., Ohta, T., & Maximov, T. C. (2014). Temporal variations in the linkage between the net ecosystem exchange of water vapour and CO_2 over boreal forests in eastern Siberia. *Ecohydrology*, *7*(2), 209–225. doi: 10.1002/eco.1449

Kotani, A., Saito, A., Kononov, A. V., Petrov, R. E., Maximov, T. C., Iijima, Y., & Ohta, T. (2019). Impact of unusually wet permafrost soil on understory vegetation and CO_2 exchange in a larch forest in eastern Siberia. *Agricultural and Forest Meteorology*, *265*, 295–309. doi: 10.1016/j.agrformet.2018.11.025

Maximov, T. C., Maksimov, A. P., Kononov, A. V., Kotani, A., & Dolman, A. J. (2019). Carbon cycles in forests. In T. Ohta, T. Hiyama, Y. Iijima, A. Kotani,

560   & T. C. Maximov (Eds.), *Water-carbon dynamics in eastern siberia* (pp. 69–

561   100). Singapore: Springer Singapore. doi: 10.1007/978-981-13-6317-7_4

562 Nelson, F. E., Hinkel, K. M., Shiklomanov, N. I., Mueller, G. R., Miller, L. L., &

563   Walker, D. A.   (1998).   Active-layer thickness in north central Alaska: Sys-

564   tematic sampling, scale, and spatial autocorrelation.   *Journal of Geophysical*

565   *Research: Atmospheres*, *103*(D22), 28963–28973. doi: 10.1029/98JD00534

566 Nelson, F. E., Shiklomanov, N. I., Hinkel, K. M., & Christiansen, H. H. (2004). The

567   circumpolar active layer monitoring (CALM) workshop and THE CALM II

568   Program. *Polar Geography*, *28*(4), 253–266. doi: 10.1080/789610205

569 Nelson, F. E., Shiklomanov, N. I., & Mueller, G. R.   (1999).   Variability of active-

570   layer thickness at multiple spatial scales, north-central Alaska, U.S.A.   *Arctic,*

571   *Antarctic, and Alpine Research*, *31*(2), 179–186.   doi: 10.1080/15230430.1999

572   .12003295

573 Ohta, T., Kotani, A., Iijima, Y., Maximov, T. C., Ito, S., Hanamura, M., . . . Maxi-

574   mov, A. P. (2014). Effects of waterlogging on water and carbon dioxide fluxes

575   and environmental variables in a Siberian larch forest, 1998–2011. *Agricultural*

576   *and Forest Meteorology*, *188*, 64-75. doi: 10.1016/j.agrformet.2013.12.012

577 Sato, H., Itoh, A., & Kohyama, T.   (2007).   SEIB–DGVM: A new Dynamic Global

578   Vegetation Model using a spatially explicit individual-based approach.   *Ecolog-*

579   *ical Modelling*, *200*(3), 279–307. doi: https://doi.org/10.1016/j.ecolmodel.2006

580   .09.006

581 Sato, H., & Kobayashi, H.   (2018).   Topography controls the abundance of siberian

582   larch forest. *Journal of Geophysical Research: Biogeosciences*, *123*(1), 106-116.

583   doi: 10.1002/2017JG004096

584 Sato, H., Kobayashi, H., Iwahana, G., & Ohta, T. (2016). Endurance of larch forest

585   ecosystems in eastern Siberia under warming trends.   *Ecology and Evolution*,

586   *6*(16), 5690-5704. doi: 10.1002/ece3.2285

587 Shin, N., Kotani, A., Sato, T., Sugimoto, A., Maximov, T. C., Nogovitcyn, A.,

588   . . . Tei, S.   (2020).   Direct measurement of leaf area index in a decidu-

589   ous needle-leaf forest, eastern Siberia.   *Polar Science*, *25*, 100550.   doi:

590   10.1016/j.polar.2020.100550

591 Shur, Y., Hinkel, K. M., & Nelson, F. E.   (2005).   The transient layer: implications

592   for geocryology and climate-change science.   *Permafrost and Periglacial Pro-*

593   *cesses*, *16*(1), 5–17. doi: 10.1002/ppp.518

594 Smith, S. L., Wolfe, S. A., Riseborough, D. W., & Nixon, F. M. (2009). Active-layer

595   characteristics and summer climatic indices, Mackenzie Valley, Northwest Ter-

596   ritories, Canada. *Permafrost and Periglacial Processes*, *20*(2), 201–220. doi:

597   10.1002/ppp.651

598 Watanabe, K., Kiyosawa, H., Fukumura, K., Ezaki, T., & Mizoguchi, M. (2003).

599   Spatial and temporal variation in thaw depth in Siberian tundra near Tiksi. In

600   M. Phillips, S. M. Springman, & L. U. Arenson (Eds.), *Permafrost (proceedings*

601   *of the eighth international conference on permafrost)* (Vol. 2, pp. 1211–1216).

602   Zurich, Switzerland.

603 Wright, N., Hayashi, M., & Quinton, W. L. (2009). Spatial and temporal vari-

604   ations in active layer thawing and their implication on runoff generation in

605   peat-covered permafrost terrain. *Water Resources Research*, *45*(5). doi:

606   10.1029/2008WR006880